

D. Mijuca · A. Žibera · B. Medjo

A novel primal-mixed finite element approach for heat transfer in solids

Received: 27 April 2005 / Accepted: 19 December 2005
© Springer-Verlag 2006

Abstract A new reliable primal–mixed finite element approach for the heat transfer analysis in solids, is examined in detail. The essential contribution is that both variables of interest, temperature and heat flux, are calculated simultaneously from the same system of finite element equations. In addition, as a novelty, continuity of the trial and test heat flux functions is enforced, to avoid the need for some a posteriori heat flux smoothing technique. In order to minimize the accuracy error and enable introduction of the flux constraints, tensorial character of the present finite element equations is fully respected. The proposed finite element is subjected to low and high order convergence and efficiency tests in steady state and transient heat transfer analysis, which enlighten its solvability, stability, accuracy and effectiveness, i.e. its reliability.

Keywords Heat transfer · Finite element method · Mixed variational · Solid mechanics · Reliability

1 Introduction

Increased thermal efficiency and integrity of materials in high–temperature environments are essential requirements in engineering structures. Therefore, either alone, or as an integral part of thermo–mechanical analysis, the heat transfer analysis is of great importance in the analysis and design of engineering components. Since analytical solutions may be found only for simple geometries, the numerical methods implemented on computers have been used for several decades. One of the first numerical methods used for this purpose is the finite difference method (FDM). It is straightforward to apply and results with system of equations that is simple to solve [1]. However, it has difficulties in treatment of irregular boundaries. Additionally, it remains intimately

tied to the grid. The analysis involves functions defined over a discrete set of points, i.e. the grid. It is derived by approximating operators.

The other method is the finite element method (FEM) [2,3]. Generally, emphasis is given to *primal* FEM, where temperature is the only one solution variable, which should satisfy the temperature boundary conditions and appropriate interelement conditions. The heat flux field is calculated a posteriori by some of recovery schemes. Unlike FDM, it can be easily lifted from the grid into a function space, everywhere in the given domain. In addition, the primary approximation step in deriving the FEM is replacing the solution by an approximation. Main advantages of the FEM over FDM are simple treatment of irregular boundaries and anisotropic materials, ability to change element size and shape in order to fit arbitrary boundaries, more natural introduction of boundary conditions, and improvement of accuracy by using higher order elements.

Alternatively, a multifield finite element method [2] is one which has more than one solution variable in the resulting formulation. If all fields of variables are of the same dimensionality the resulting multifield approach is called *mixed*, otherwise it is called *hybrid*. Mixed formulations reduce the order of differential equation and therefore its continuity requirement. Other advantages of mixed over primal finite element approaches are their robustness in the presence of limiting and extreme situations, like irregular boundaries and non–smooth boundary conditions. Nevertheless, since there are at least two fundamental variables, the overall stability of mixed approaches is not easy to achieve. Another consequence is that resulting system matrix is not positive definite, as in primal approaches, which raise the need for specially designed technique for solution of large-scale systems of linear equations [4,5]. Further, the boundary element (BEM) formulation [6] is more attractive as a small scale, high order approximation. In addition, meshless methods are also used [7,8]. They are simple to implement, accurate and require no polygonalisation of the domain. Weakness of these methods is that they require much more computational time to achieve convergence of the results.

D. Mijuca (✉) · A. Žibera · B. Medjo
Department of Mechanics, Faculty of Mathematics,
University of Belgrade, Belgrade Serbia and Montenegro
E-mail: dmijuca@matf.bg.ac.yu
Tel.: +381-11-20-27-801
Fax: +381-11-630-151

On the other hand, analysis of transient heat flow involves conduction heat transfer in regions of arbitrary shape where temperature is a function of both time and position. The most usual numerical approach is to separate discretization procedure for space and time variables [9]. The time is usually discretized using the FDM, while the space is discretized either by the FEM, or by some other numerical method. By discretization of the starting problem using FEM, a system of semi-discrete initial value problems is obtained, which can be solved by various methods, for example θ -method. By changing the parameter θ , well-known finite difference schemes are obtained, like Crank-Nicholson ($\theta = 1/2$), Euler forward ($\theta = 0$), Euler backward ($\theta = 1$) or Galerkin ($\theta = 2/3$). It is also possible to apply multistep schemes for time discretization [9]. Since transient heat transfer problem is a parabolic problem, it is possible to solve it using either explicit or implicit time schemes. The explicit methods are only conditionally stable, requiring the time-step to be restricted below a certain critical value to maintain numerical stability. The maximum time-step allowed is governed by the largest eigenvalue of the problem. On the other hand, implicit finite difference schemes are unconditionally stable, although they require much more computational effort than the explicit time schemes. Another available method is the fundamental collocation method [10,11].

In this paper, a new reliable fully three-dimensional primal-mixed finite element approach for the solution of steady state and transient heat transfer in solids, is examined in detail. It has two solution variables that are simultaneously calculated: temperature and heat flux. As a novelty, the inter-element continuity of the heat flux shape functions is intentionally enforced. Consequently, the need for some a posteriori scheme [12] for the recovery of the heat flux field is avoided. Implicit Euler backward time scheme is used in order to obtain the stable solution during the time integration. Further, the well-known transition problem, that is, connecting finite elements of different dimensionality in situation where model problem has geometrical transitions from solid to thick or thin, is avoided by the use of robust hexahedral finite elements only. The main motive for this development is found in lack of hexahedral (solid) finite element that is reliable and robust [13,14], and which can be reliably used in the subsequent mechanical analysis. Hence, the main goal is to prove the reliability of the approach proposed by the low and high order convergence tests. The future investigation is oriented toward implementation of the present approach in the semi-coupled thermo-mechanical code, where original primal-mixed finite element elasticity analysis is introduced in [15]. Namely, the new approach will be oriented for more accurate determination of thermal stresses, where no consistency problem [16] will occur in calculation of thermal and mechanical deformations. The possible areas of application are in the analysis and design of standard engineering structures, as well as in advanced analyses of thermal barrier coatings (turbine blades), micro electronic packages, multi-scale phenomena and analyses of freezing and thawing of human organs.

2 Primal-mixed formulation of the heat transfer

The mathematical model of transient heat transfer in solids is based on conservation principle (1) and constitutive law (2), in strong form [8,10]:

$$\rho c \frac{\partial T}{\partial t} + \text{div} \mathbf{q} - f = 0 \quad \text{in} \Omega \quad (1)$$

$$\mathbf{q} = -\mathbf{k} \nabla T \quad \text{in} \Omega. \quad (2)$$

In above expressions, the state of the body is described by temperature T and heat flux vector \mathbf{q} . The body has three material properties k , ρ and c . The quantity k is a second order tensor of thermal conductivity, in general case, of an orthotropic material. If the material is homogeneous and isotropic, the tensor k will degenerate to simple scalar value k , i.e. thermal conductivity. Further, ρ is the material density, and c is the specific heat, while f stands for the internal heat source generated per unit volume. It is presently assumed that material properties are independent of the temperature. In addition, variables $T(X, t)$, $\mathbf{q}(X, t)$, $f(X, t)$ are functions of the space X and time t . Further, $\bar{\Omega}$ is some closed and bounded domain of the Euclidian space E^n ($n = 1, 2, 3$) occupied by the considered body. Inner part of $\bar{\Omega}$ is denoted by Ω , and its boundary by $\partial\Omega$, $\Omega \cup \partial\Omega = \bar{\Omega}$. The boundary is subdivided into four parts: $\partial\Omega_T, \partial\Omega_q, \partial\Omega_c$ and $\partial\Omega_r$, which are: the part of the boundary per temperature, per prescribed heat flux, heat flux due to the prescribed convection and heat flux due to the prescribed radiation, respectively, such that $\partial\Omega_T \cup \partial\Omega_q \cup \partial\Omega_c \cup \partial\Omega_r = \partial\Omega$.

In order to obtain unique solution of the above equations, the following set of essential boundary conditions per temperature (3) and boundary conditions per heat flux (4)–(6), are available:

$$T = \bar{T} \quad \text{on} \partial\Omega_T, \quad (3)$$

$$\mathbf{q} \cdot \mathbf{n} = q_h = h \quad \text{on} \partial\Omega_q, \quad (4)$$

$$\mathbf{q} \cdot \mathbf{n} = q_c = h_c(T - T_a) \quad \text{on} \partial\Omega_c, \quad (5)$$

$$\mathbf{q} \cdot \mathbf{n} = q_r = h_r \sigma A(T^4 - T_a^4) \quad \text{on} \partial\Omega_r, \quad (6)$$

Specifically, Neumann boundary conditions due to the prescribed heat flux are given by the expression (4). While, Robin boundary conditions due to the prescribed convection are given by the expression (5), where h_c is the convection coefficient and T_a is the ambient (environmental) temperature. And finally, boundary conditions per radiation are given by (6). The initial boundary conditions are given by $T|_{t=0} = T_0$. If heat transfer is independent of time, the first term in (1) vanishes, and problem reformulates to steady-state heat transfer.

The boundary condition (3) is essential, and hence exactly satisfied by the trial functions of the problem. Therefore, we need to consider only the weak forms of the equations (1) and (2). Using the Galerkin procedure, one can seek the weak solution of (1):

$$\int_{\Omega} \left(\rho c \frac{\partial T}{\partial t} + \text{div} \mathbf{q} - f \right) \theta d\Omega = 0 \quad (7)$$

where θ denotes test functions in the complete space of interpolation functions, which are taken from the Hilbert space L_2 of all real measurable square integral scalar functions: $\int_{\Omega} g^2 d\Omega < \infty$, with the inner product $(h, g) = \int_{\Omega} hgd\Omega$ and norm defined by $\|g\|^2 = (g, g)$ for all $h, g \in L_2(\Omega)$.

Further, the weak form of the inverted constitutive equation (2), where vector Q is the test function taken from the space of all measurable square integrable vector fields is given by:

$$\int_{\Omega} (k^{-1}\mathbf{q} + \nabla T)Qd\Omega = 0 \quad (8)$$

Simple summation of (7) and (8) gives us the expression which represents an asymmetric weak formulation of the mixed problem.

Find $\{T, \mathbf{q}\} \in H^1(\Omega) \times H(\text{div})$ satisfying boundary conditions and

$$\int_{\Omega} (k^{-1}\mathbf{q} + \nabla T)Qd\Omega = \int_{\Omega} \left(\rho c \frac{\partial T}{\partial t} + \text{div } \mathbf{q} - f \right) \theta d\Omega \quad (9)$$

for all $\{\theta, \mathbf{Q}\} \in L_2(\Omega) \times L_2(\Omega)$.

In these expressions, space $H(\text{div})$ is the space of all vector fields which are square integrable and have square integrable divergence. However, asymmetric formulations are impractical from the computational point of view. Integrating by parts and applying the divergence theorem on the first term on the right side of (9) yields symmetric weak form of the mixed problem, where H^1 is the space of all scalar fields which are square integrable and have square integrable gradients, with the norm $\|g\|^2 = \int_{\Omega} ((g')^2 + g^2)d\Omega$ for all

$g \in H^1(\Omega)$:

Find $\{T, \mathbf{q}\} \in H^1(\Omega) \times L_2(\Omega)$ such that $T|_{\partial\Omega_T} = \bar{T}$ and

$$\begin{aligned} & \int_{\Omega} \mathbf{q}\mathbf{k}^{-1}Qd\Omega + \int_{\Omega} \nabla T \cdot Qd\Omega \\ &= \int_{\Omega} \rho c \frac{\partial T}{\partial t} \theta d\Omega + \int_{\Omega} \mathbf{q} \cdot \nabla \theta d\Omega - \int_{\Omega} \theta f d\Omega \\ & - \int_{\partial\Omega_q} \theta h d\Omega - \int_{\partial\Omega_c} q_c \theta d\Omega \end{aligned} \quad (10)$$

for all $\{\theta, \mathbf{Q}\} \in H^1(\Omega) \times L_2(\Omega)$ such that $\theta|_{\partial\Omega_T} = 0$.

As an essential contribution of the present approach, the trial and test shape functions for the heat flux variable are presently chosen from continuous subspace H^1 , instead from space L_2 . It is done in order to enforce interelement continuity of the heat flux field over the subdomains of the body, where it is physically justified.

In the present approach, the Backward Euler scheme [9], for which holds:

$$\rho c \frac{\partial T}{\partial t} \Big|_n \approx \rho c \frac{nT - n^{-1}T}{\Delta t} \quad (11)$$

is used for the time discretization.

2.1 Finite element approximation

Let C_h be the partitioning of the domain Ω into elements Ω_i . Let us define finite element subspaces for the temperature T , the heat flux vector q and the appropriate test (weight) functions, respectively as:

$$\begin{aligned} T_h &= \left\{ T \in H^1(\Omega) : T|_{\partial\Omega_T} = \bar{T}, \quad T = T^L P_L(\Omega_i), \quad \forall \Omega_i \in C_h, \right\} \\ \theta_h &= \left\{ \theta \in H^1(\Omega) : \theta|_{\partial\Omega_T} = 0, \quad \theta = \theta^M P_M(\Omega_i), \quad \forall \Omega_i \in C_h, \right\} \\ Q_h &= \left\{ q \in H^1(\Omega) : q \cdot \mathbf{n}|_{\partial\Omega_q} = h, \quad q \cdot \mathbf{n}|_{\partial\Omega_c} = h_c(T - T_0), \right. \\ & \quad \left. q = q^L V_L(\Omega_i), \quad \forall \Omega_i \in C_h, \right\} \\ \vartheta_h &= \left\{ Q \in H^1(\Omega) : Q \cdot \mathbf{n}|_{\partial\Omega_q \cup \partial\Omega_c} = 0, \right. \\ & \quad \left. Q = Q^M V_M(\Omega_i), \quad \forall \Omega_i \in C_h, \right\} \end{aligned} \quad (12)$$

In these expressions T^L and q^L are nodal values of the temperature scalar T and flux vector \mathbf{q} , respectively. Accordingly, P_L and V_L are corresponding values of the interpolation (shape, local base) functions connecting temperatures and fluxes at an arbitrary point in Ω_i (the body of an element), and the nodal values of these quantities. The complete analogy holds for the temperature and flux weight functions θ and Q .

Heat flux approximation functions are presently chosen from continuous subspace H^1 , instead from space L_2 . It should be noted that number of numerical experiments reported here reveals that this local violation of discontinuity on the interfaces of abrupt material changes and over the part of the boundary where non-smooth heat flux boundary conditions are prescribed, does not deteriorate results.

Let n_T be the number of temperature degrees of freedom, and n_q the number of heat flux degrees of freedom. By analogy with finite element approach in elasticity [16], the present scheme can be written as a system of linear equations of order $n = n_q + n_T$. In matrix form at current time t , it reads:

$$\begin{aligned} & \begin{bmatrix} A_{vv} & B_{vv}^T \\ B_{vv} & -D_{vv} - S_{vv} \end{bmatrix} \begin{bmatrix} q_v \\ T_v \end{bmatrix} \\ &= \begin{bmatrix} -A_{vp} & -B_{vp}^T \\ -B_{vp} & D_{vp} \end{bmatrix} \begin{bmatrix} q_p \\ T_p \end{bmatrix} + \begin{bmatrix} 0 & 0 \\ 0 & S_{vp} \end{bmatrix} \begin{bmatrix} 0 \\ T_p^{(t-1)} \end{bmatrix} \\ & + \begin{bmatrix} 0 \\ F_p + H_p - K_p \end{bmatrix} + \begin{bmatrix} 0 \\ -L_p^{(t-1)} \end{bmatrix} \end{aligned} \quad (13)$$

In this expression, unknown (variable) and known (initial, prescribed) values of the heat flux and temperature, denoted by the indices v and p , respectively, are decomposed. The nodal heat flux (q^{pL}) and temperature (T^L) components are consecutively ordered in the column matrices q , and T , respectively. The nonhomogenous essential boundary conditions or initial boundary conditions per temperature T_p and heat flux q_p (providing that their relevant part of the boundaries do not intersect) are introduced as contribution to the right-hand side of the expression (13). The members of the entry matrices A , B , D and S , and the column matrices F ,

H , K and L in (13), are respectively:

$$\begin{aligned}
 A_{\Lambda p \Gamma r} &= \sum_e \int_{\Omega_e} \Omega_{\Lambda}^L g_{(L)p}^a V_L k_{ab}^{-1} g_{(M)r}^b V_M \Omega_{\Gamma}^M d\Omega_e, \\
 B_{\Lambda p \Gamma} &= \sum_e \int_{\Omega_e} \Omega_{\Lambda}^L g_{(L)p}^a V_L P_{M,a} \Omega_{\Gamma}^M d\Omega_e, \\
 D_{\Lambda \Gamma} &= \sum_e \int_{\partial \Omega_{ce}} h_c \Omega_{\Lambda}^L P_L P_M \Omega_{\Gamma}^M \partial \Omega_{ce}, \\
 F_{\Gamma} &= \sum_e \int_{\Omega_e} \Omega_{\Gamma}^M P_M f d\Omega_e, \\
 S_{\Lambda \Gamma} &= \sum_e \int_{\Omega_e} \frac{\rho c}{\Delta t} \Omega_{\Lambda}^L P_L P_M \Omega_{\Gamma}^M d\Omega_e, \\
 L_{\Gamma} &= \sum_e \int_{\Omega_e} \frac{\rho c}{\Delta t} T_{(M)}^{n-1} P_M \Omega_{\Gamma}^M d\Omega_e, \\
 H_{\Gamma} &= \sum_e \int_{\partial \Omega_{he}} \Omega_{\Gamma}^M P_M h d \partial \Omega_{he}, \\
 K_{\Gamma} &= \sum_e \int_{\partial \Omega_{ce}} \Omega_{\Gamma}^M P_M h_c T_a d \partial \Omega_{ce}. \tag{14}
 \end{aligned}$$

The above expressions should be evaluated for each unsuppressed degree of freedom of the heat flux vector or temperature, connected to the global node Λ and/or Γ of the

considered finite element mesh, where Ω_{Λ}^L is connectivity operator, which maps the set of global nodes Λ into the set of local nodes L per elements, and vice versa. The Euclidian shifting operator $g_{(L)p}^a$ is given by $g_{(L)p}^a = \delta_{ij} g^{ac} (\partial z^i / \partial \xi^c)$ ($\partial z^j / \partial y^{(L)p}$), where, z^i ($i, j, k, l = 1, 2, 3$) is global Cartesian coordinate system of reference. The coordinate system at each local node L is denoted by $y^{(L)r}$ ($r, s, t = 1, 2, 3$). The local natural (convective) coordinate system per finite element is denoted by ξ^a ($a, b, c, d = 1, 2, 3$). Further, g^{ab} and $g^{(L)mn}$ are components of the contravariant fundamental metric tensors, per natural ξ^a and local $y^{(L)n}$ coordinate systems, respectively. Furthermore, $P_{M,a} \equiv \partial P_M / \partial \xi^a$. Since tensorial character is fully respected, one can easily choose appropriate coordinate system at each global node for prescribing of heat flux, or interpretation of the results.

2.2 Finite element configurations

The topology of the present hexahedral continuous finite element family HCT/q for approximation of temperature and heat flux fields is shown in Fig. 1. It contains 8 or 20 local nodes for approximation of temperature, and 9–27 local nodes for the approximation of the heat flux.

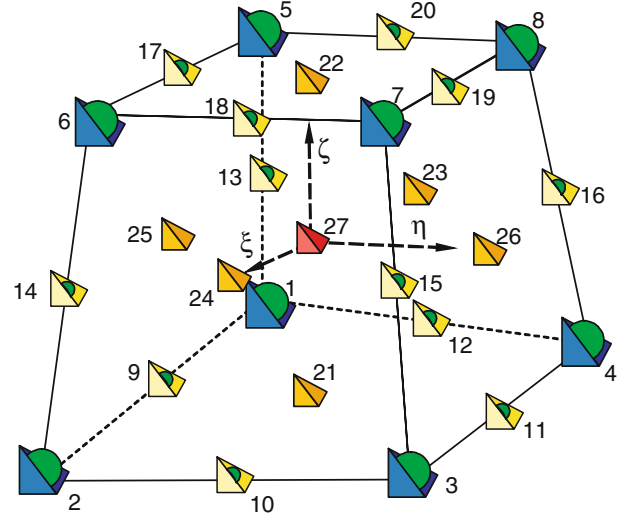


Fig. 1 Finite element HC (8 - 20)/(20-27)

If there are eight local nodes per temperature, the corresponding shape functions are tri-linear, given by:

$$P_i = \frac{1}{8} (1 + \xi_i \xi) (1 + \eta_i \eta) (1 + \zeta_i \zeta), \quad \text{for nodes } i = 1, 8 \tag{15}$$

In this case, heat flux is represented by 9 nodes (finite element HC8/9), 15 nodes (HC8/15), or 27 nodes (HC8/27), connected to the 9, 15, or 27 shape functions, respectively. That is, 1, 7 or 19 nodes more than for approximation of the temperature, respectively.

On the other hand, if there are 20 local nodes per temperature, the relevant shape functions are of serendipity type, given by:

$$\begin{aligned}
 P_i &= \frac{1}{8} (1 + \xi_i \xi) (1 + \eta_i \eta) (1 + \zeta_i \zeta) \\
 &\quad (\xi_i \xi + \eta_i \eta + \zeta_i \zeta - 2), \quad \text{for nodes } i = 1, 8, \\
 P_i &= \frac{1}{4} (1 - \xi^2) (1 + \eta_i \eta) (1 + \zeta_i \zeta), \quad \text{for nodes } i = 9, 11, 17, 19, \\
 P_i &= \frac{1}{8} (1 + \xi_i \xi) (1 - \eta^2) (1 + \zeta_i \zeta), \quad \text{for nodes } i = 10, 12, 18, 20, \\
 P_i &= \frac{1}{8} (1 + \xi_i \xi) (1 + \eta_i \eta) (1 - \zeta^2), \quad \text{for nodes } i = 13, 14, 15, 16. \tag{16}
 \end{aligned}$$

In this case heat flux is approximated by 21 nodes (HC20/21) or 27 nodes (HC20/27), which are connected to 21 or 27 shape functions, respectively. That is, 1 or 7 nodes more than for approximation of the temperature. Shape functions given by (15) and (16) are complete up to the order of polynomials $m = 1$, fulfilling the completeness requirements for our formulation

It can be seen that the subspaces for approximation of the heat flux field are enriched in accordance to the temperature field. The additional shape functions are *hierarchical* in order to increase stability. It will be shown, that only finite element HC8/27 is reliable [14].

2.3 Solution of the resulting system of equations

The modified direct MA47 solution procedure, particular version of the Duff–Reid algorithm [4,5], which solves a sparse symmetric indefinite system of linear equations using multifrontal Gaussian elimination and makes a special effort to exploit zero diagonal entries, is presently used. In order to increase the robustness of the solution procedure even in the case of geometrically multiscale analyses the scaling routine MC30 [17] is included, also. The performance of this solution approach is studied and compared with existing in-house sparse Gaussian elimination solver (SSGE). The numerical examples were run on the PC Pentium IV 2.4GHz 2GB RAM and NEC supercomputer SX6i 8GB RAM. It will be shown here that MA47+MC30 program routine is two orders of magnitudes faster than SSGE routine. Obtained numerical results confirmed the time efficiency and reliability of the MA47+MC30 solution approach.

3 Primal formulation of the heat transfer

The primal finite element approach in steady state heat transfer analysis [10], presently used for comparison, is given by the next matrix equation:

$$[C_{vv}+D_{vv}][T_v] = -[C_{vp}+D_{vp}][T_p] + [-F_p - H_p + K_p], \quad (17)$$

where all block matrix entries are the same as in (14), except for the block matrix C , which is for every pair of nodes (Λ, Γ) calculated by:

$$C^{\Lambda\Gamma} = \sum_e \int_{\Omega_e} \Omega_L^{\Lambda} P_{,a}^L k^{ab} P_{,d}^M \Omega_M^{\Gamma} d\Omega_e. \quad (18)$$

If corresponding finite element has 8 or 20 local nodes, connected to the shape functions given by (15) or (16), the resulting finite element scheme is called *raw* and presently denoted by H8 or H20, respectively.

4 Low order tests

In order to check necessary and sufficient conditions for convergence, low order tests are traditionally the first steps in the validation process of each new finite element. In addition, some authors considered these tests as tools for assessment of robustness of finite element algorithms [14]. In the present paper, necessary [12] and sufficient conditions [18, 19] solvability tests are investigated in detail.

4.1 Necessary conditions for solvability

The single finite element configuration passes solvability test if the number of heat flux degrees of freedom n_q is greater than the number of temperature degrees of freedom n_T . This

Table 1 Necessary conditions for solvability test

FE configuration	n_T	n_q	$n_T + n_q$	Test $n_q > n_T$
HC8/8	8	24	32	Pass
HC8/9	8	27	35	Pass
HC8/15	8	45	53	Pass
HC8/27	8	81	89	Pass
HC20/20	20	60	80	Pass
HC20/21	20	63	83	Pass
HC20/27	20	81	101	Pass

test is known [12] as the single element patch test, or necessary condition for solvability. The results of the present test are reported in Table 1. It can be seen that all considered finite element configurations satisfy this requirement.

4.2 Sufficient conditions for solvability. Eigenvalue analysis

In order to check if one finite element is sensitive to the locking phenomena, an eigenvalue analysis of single finite element configuration, is performed [15,18]. This test is also known as sufficient conditions for solvability test. In the present context, one finite element free of boundary conditions passes this test if number of zero eigenvalues of the system matrix in (13) is equal to one. In addition, there should be $n_T - 1$ negative eigenvalues and one (almost) zero eigenvalue which correspond to the temperature degrees of freedom (dof), and n_q positive eigenvalues that correspond to the heat flux dof.

The results of the present test for all considered finite element configurations: HC8/9, HC8/15, HC8/27, HC20/21 and HC20/27, are reported in Tables 2 and 3. Calculated eigenvalues are sorted in increasing order. All eigenvalues connected to the temperature dof are reported, whilst only the smallest and the largest eigenvalue connected to the heat flux dof are reported. It can be seen that all finite element configurations presently considered pass the sufficient conditions for solvability test.

5 High-order tests: the mathematical convergence requirements

As the finite element mesh is refined, the solution of discrete problem should converge to the analytical solution of the mathematical model. The convergence requirements for shape functions are grouped into three categories, that is: completeness, compatibility and stability [13–15]. Completeness criterion requires that polynomial order of finite element approximation functions must ensure that all integrals in the corresponding weak formulation are finite. Specifically, if m is variational index calculated as the highest spatial derivative order that appears in the energy functional of the relevant boundary value problem, than shape functions must represent exactly all polynomial terms in order $\leq m$ in element coordinate system. A set of shape functions that

Table 2 Eigenvalues of one finite element configurations HC8/(8–27)

Mode (dof)		HC8/8	HC8/9	HC8/15	HC8/27
1		-1.951941E-01	-2.290541E-01	-2.868752E-01	-3.303563E-01
2		-1.951941E-01	-2.290541E-01	-2.868752E-01	-3.303563E-01
3		-1.951941E-01	-2.290541E-01	-2.868752E-01	-3.303563E-01
4	Temp	-9.884506E-02	-9.884506E-02	-1.224534E-01	-1.560596E-01
5		-9.884506E-02	-9.884506E-02	-1.224534E-01	-1.560596E-01
6		-9.884506E-02	-9.884506E-02	-1.224534E-01	-1.560596E-01
7		-4.166667E-02	-4.166667E-02	-4.166667E-02	-5.384102E-02
8		-1.173784E-016	-4.937518E-017	-6.245006E-017	-7.209485E-018
9		4.629630E-03	4.629630E-03	1.594840E-003	9.093757E-05
10-31		...			
32		3.201941E-01	...		
33-34				...	
35	Flux		4.685373E-01		
36-52					
53				9.008513E-01	
54-88					
89				1.290335E+00	

Table 3 Eigenvalues of one finite element configurations HC20/(20–27)

Mode (dof)		HC20/20	HC20/21	HC20/27
1		-5.2741227E-01	-5.6288920E-01	-6.4052454E-01
2		-5.2741227E-01	-5.6288920E-01	-6.4052454E-01
3		-5.2741227E-01	-5.6288920E-01	-6.4052454E-01
4		-4.6939502E-01	-4.6939502E-01	-5.4653861E-01
5		-2.8229067E-01	-2.8229067E-01	-3.2452143E-01
6		-2.8229067E-01	-2.8229067E-01	-3.2452143E-01
7		-1.3914343E-01	-1.3914343E-01	-1.5839084E-01
8		-1.3914343E-01	-1.3914343E-01	-1.5839084E-01
9	Temp	-1.3914343E-01	-1.3914343E-01	-1.5839084E-01
10		-8.2290600E-02	-8.2290600E-02	-8.8105436E-02
11		-8.2290600E-02	-8.2290600E-02	-8.8105436E-02
12		-8.2290600E-02	-8.2290600E-02	-8.8105436E-02
13		-4.4507986E-02	-4.6499991E-02	-4.7320591E-02
14		-4.4507986E-02	-4.6499991E-02	-4.7320591E-02
15		-4.4507986E-02	-4.6499991E-02	-4.7320591E-02
16		-4.1170916E-02	-4.1170916E-02	-4.1170916E-02
17		-2.6149094E-02	-2.6149094E-02	-2.6390235E-02
18		-2.6149094E-02	-2.6149094E-02	-2.6390235E-02
19	-2.6149094E-02	-2.6149094E-02	-2.6390235E-02	
20		5.0611788E-17	-1.9021935E-17	-7.0748837E-17
21		2.2326639E-03	2.0611104E-03	1.4085152E-04
22-79		...		
80		1.0261153E+00	...	
81-82	Flux			...
83			1.1915502E+00	
85-100				
101				1.6450622E+00

satisfies this condition is called m -complete. Further, compatibility criterion requires that shape functions should provide continuity of primal variable between elements. Thus, patch trial functions must be C^{m-1} continuous between interconnected elements, and C^m piecewise differentiable inside each element. A finite element model that passes both completeness and continuity requirements satisfies consistency condition between mathematical and discrete models.

The overall stability of mixed formulations is provided if two necessary conditions for stability are fulfilled: the first stability condition represented by the ellipticity on the kernel, and second stability condition represented by the inf-sup test [14]. For example, in dual-mixed methods [13], the first stability condition requires that space for the approximation

of primal variable is large enough compared to the space for approximation of dual variable, while the second stability condition requires just the opposite. Obviously, these two conditions are in contradiction. Thus, the well balance between these approximation spaces must be established in order to avoid instabilities [20]. It is shown in [13] and [15] that for primal-mixed methods, where interelement continuity on the dual approximation spaces is enforced and test and trial functions are identical (like in the present case) it is straightforward to achieve stability.

The Lax-Wendroff theorem says that consistency and stability imply convergence. It should be noted that satisfaction of the completeness criterion is necessary for convergence of the finite element solutions, while violating other two criteria does not necessary means that solution will not converge.

5.1 Consistency condition for FE HC(8–20)/(9–27)

Presently, variational indices for temperature and heat flux variable fields are $m = 1$ and $m = 0$, respectively. Nevertheless, all test and trial shape functions are presently chosen from space H^1 , i.e. from the class of C^0 -continuous shape functions, given by (15) and (16). Consequently, the completeness and compatibility requirements for both fields are satisfied in the present case.

5.2 First stability condition

In mixed formulation, the first stability condition is satisfied if the bilinear form $a(\mathbf{q}, \mathbf{Q}) = \int_{\Omega} \mathbf{q} \mathbf{k}^{-1} \mathbf{Q} d\Omega$ is coercive on the space of the variable \mathbf{Q} [21], that is $a(\mathbf{Q}, \mathbf{Q}) \geq \alpha \|\mathbf{Q}\|^2$ for all $\mathbf{Q} \in L_2$, $\alpha \geq 0$, which is presently trivially satisfied. Hence, all presently considered finite element configurations HC(8–20)/(9–27) satisfy first stability condition a priori. In addition, the stability is automatic for all coercive methods where test and trial spaces are identical [21], as in the present case, and it is enough to enrich the dual variable space in order to increase stability.

5.3 Second stability condition

To obtain a stable and optimal procedure for the selected interpolation, a mixed formulation should also satisfy the second stability condition, so-called the inf-sup test [21]. The second stability condition is satisfied if the inf-sup parameter γ_h [14,15,21], remains bounded above zero for meshes of increasing density:

$$\gamma \leq \gamma_h = \inf_{\theta \in H^1} \sup_{Q_h \in (H^1)^n} \frac{b(Q_h, \theta_h)}{\|Q_h\| \|\theta_h\|}, \quad (19)$$

where presently:

$$b(Q_h, \theta_h) = \sum_e \int_{\Omega_i} Q_h \cdot \nabla \theta_h d\Omega_e, \quad (20)$$

$$\|Q_h\|^2 = \sum_e \int_{\Omega_i} Q_h^T \cdot Q_h d\Omega_e, \quad (21)$$

$$\|\theta_h\|^2 = \sum_e \int_{\Omega_i} \nabla \theta_h \nabla \theta_h d\Omega_e. \quad (22)$$

Since this verification involves an infinite number of meshes, inf-sup test can not be performed analytically. Therefore, it is performed numerically [21] for a limited number of meshes of increasing refinement. Consequently, numerical *inf-sup* test is represented by generalized eigenvalue problem, in matrix notation given by

$$BA^{-1}B^T x = \lambda C x, \quad (23)$$

where B and A are the block matrix entries in (13), while block matrix C is the system matrix of the primal approach (18).

Thus, the inf-sup value $\gamma_h = (\lambda_{\min})^{1/2}$ is the square root of the smallest eigenvalue of the problem (22). Some considered finite element configuration passes the inf-sup test if values γ_h do not show decrease toward zero, during the mesh refinement process.

6 Inf-sup numerical tests

The inf-sup test for the present three-dimensional finite element configurations HC(8–20)/(21–27), is performed in different limit scenarios [14], such as highly distorted finite element mesh and small thickness of plates and shells. The results are plotted in the form $\log(\gamma_h) = f(1/N)$, where $N = 1, \dots, 8$ is the number of finite elements per side. Results for meshes of increasing refinement will be plotted from right to left. It should be noted that decreasing of the inf-sup values on log-log diagram would be seen as a curve with moderate or excessive slope, which indicates that stability test is failed. It is proven in [15,22] that finite elements QC4/9 and HC8/27 are stable in linear elasticity. Presently it will be shown that finite element HC8/27 is stable in the heat transfer analysis, also.

6.1 Unit square block

The inf-sup test results for the unit square block, with thermal conductivity $k = 1$, are shown in the Fig. 2. Four finite element configurations with the mesh indicator $N = 1, 2, 3, 4$, are considered.

The inf-sup test results for the unit square block discretized by moderately distorted finite element meshes with mesh indicator $N = 1, 2, 3, 4$, are shown in the Fig. 3.

From the results shown in Fig. 2 and 3, it can be seen that only finite element configuration HC8/27 passes the inf-sup test.

6.2 Thin plate

A thin unit square plate of thickness $t = 0.01$ and thermal conductivity $k = 1$, is discretized by the sequence ($N \times N \times 1$, $N = 2, 4, 6, 8, 10$) of undistorted, moderately distorted and highly distorted hexahedral finite element meshes [14].

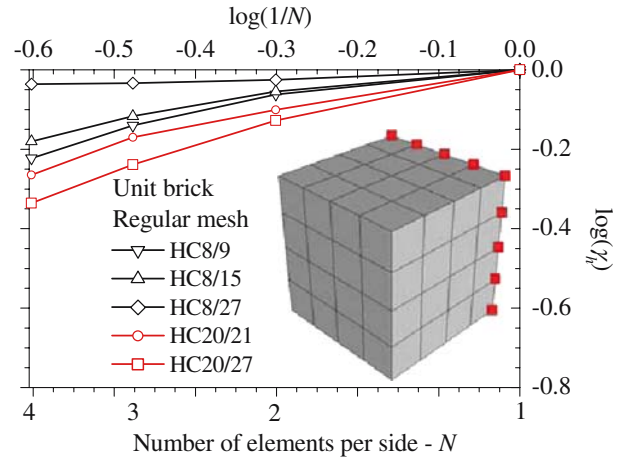


Fig. 2 Unit brick with undistorted mesh: inf-sup values

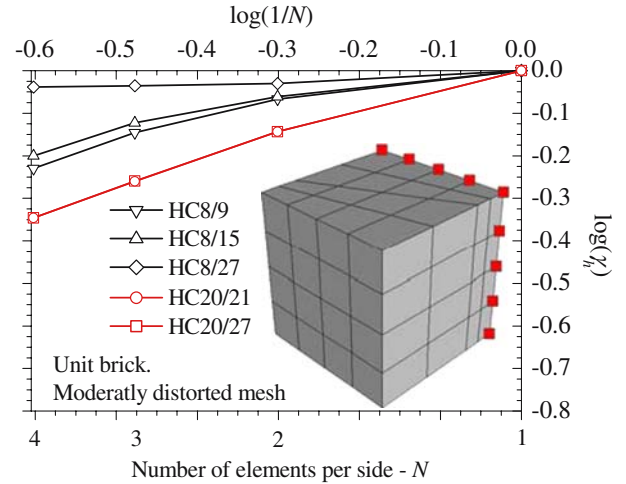


Fig. 3 Unit brick with distorted mesh: inf-sup values

Only temperature boundary conditions are imposed on one side of the model problem (see Fig. 5).

The inf-sup test results for thin plate discretized by uniform mesh are shown in Fig. 4.

The inf-sup test results for thin plate discretized by the sequence of moderately distorted finite element meshes are shown in Fig. 5.

The inf-sup test results for thin plate discretized by the sequence of highly distorted finite element meshes are shown in Fig. 6. The inf-sup results for finite element configurations HC8/15 and HC8/27, are reported.

The oscillation of the stability constants γ_h is due to the nonsimilarity of the sequence of finite element meshes considered. However, it stabilizes in the mesh refinement pro-

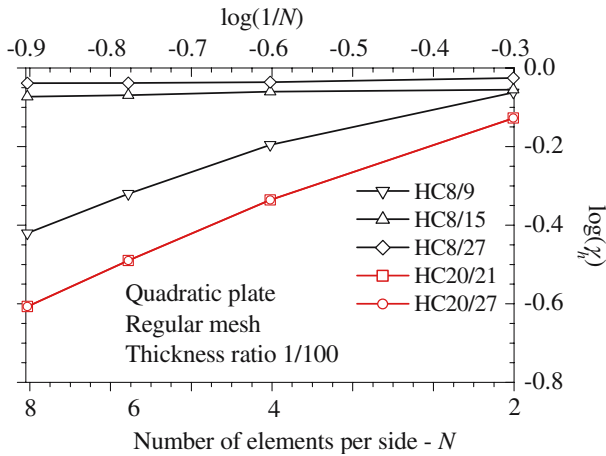


Fig. 4 Thin 3D plate with undistorted mesh: inf-sup test

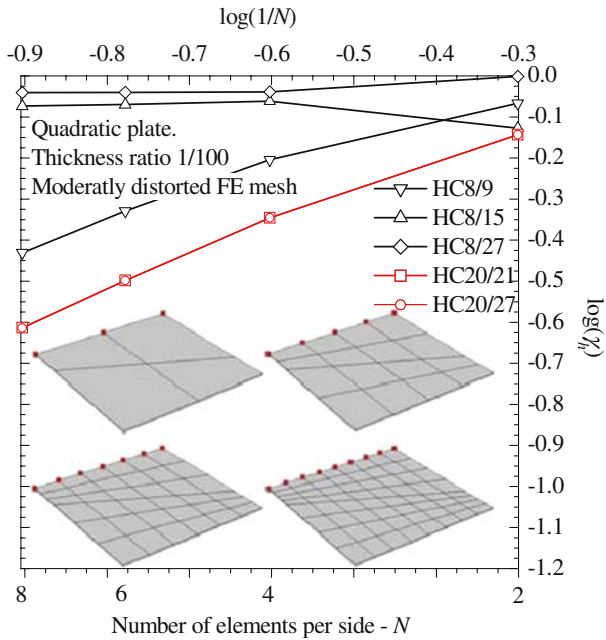


Fig. 5 Thin 3D plate with moderately distorted mesh: inf-sup values

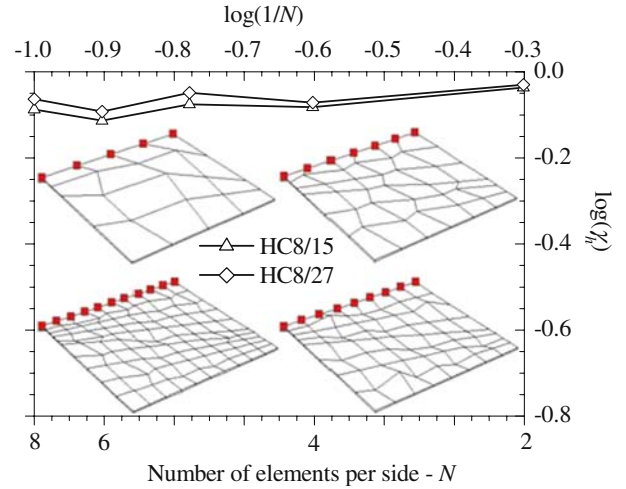


Fig. 6 Thin 3D plate with moderately distorted mesh: inf-sup values

cess. Therefore, finite elements HC8/15 and HC8/27 pass the inf-sup test in the present example.

6.3 Thin cylinder

The finite element HC8/27 is presently tested for its stability on the example of the thin cylinder model problem. The cylinder radius is $r = 1$, full length is $l = 1$ and its thickness is $t = 1/100$, while thermal conductivity is $k = 1$. The temperature is prescribed on the bottom side of the cylinder. The heat flux boundary conditions are not prescribed. Because of symmetry, only one half of the cylinder is analyzed, and only one layer of finite elements is placed along the thickness. The four finite element models with mesh indicator $N = 2, 4, 6, 8$ are considered. From the Fig. 7 we may see that only finite elements HC8/15 and HC8/27 pass the inf-sup test.

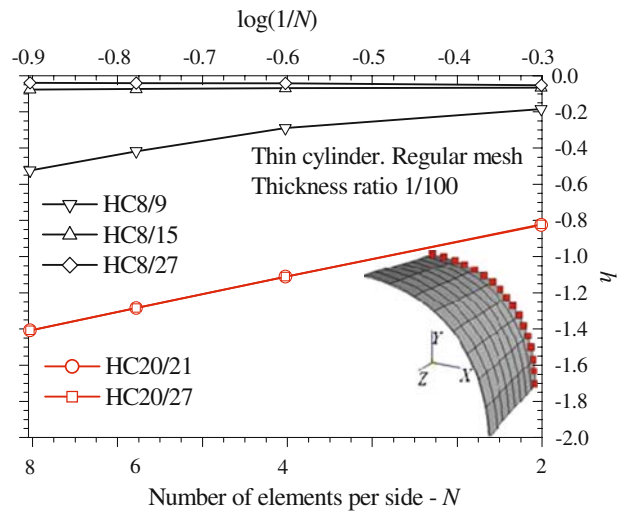


Fig. 7 Thin 3D plate with highly distorted mesh: inf-sup values

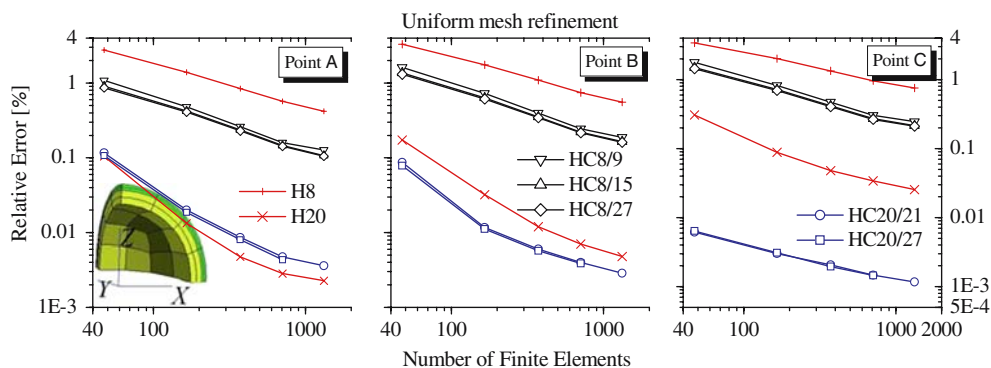


Fig. 8 Thin 3D shell with undistorted mesh: inf–sup values

From Fig. 7 it can be seen that finite elements HC8/15 and HC8/27 pass the inf–sup test. Nevertheless, finite element HC8/15 did not pass the inf–sup test in previous model problem of unit brick, so generally it can not be considered as stable one. On the other hand, finite element HC8/27 passes the test in all considered examples and it can be considered stable.

7 Numerical experiments

The proposed primal–mixed formulation was implemented in an original computer code for three–dimensional problems using the ‘Fortran’ programming language. It is tested on several verification examples in steady state and transient heat transfer analysis, with aim to study its performance in various kinds of limit situations, such as: material interface, non–smoothness of heat flux boundary conditions and thermal coating barriers. In addition, its performance in the case of orthotropic material and internal heat generation, is also inspected.

Standard relative percentage error analysis is performed in order to check how the error depends on a combination of the approximation properties of both temperature and heat flux finite element spaces.

7.1 Hollow sphere with two materials and convective BCs

Sensitivity of the present approach to the presence of the material discontinuity is investigated in the present example. A model problem is the steady state heat transfer through a hollow bimaterial sphere [23]. Inner, interfacial and outer radius of the hollow sphere are 0.3, 0.35, and 0.37 m, respectively. The convection boundary conditions are prescribed on its inner and outer surface, such that $h_c^{inner} = 200 \text{ W}/(\text{m}^2\text{C})$ and $T_a^{inner} = 70^\circ\text{C}$, and $h_c^{outer} = 150 \text{ W}/(\text{m}^2\text{C})$ and $T_a^{outer} = -9^\circ\text{C}$, respectively. Thermal conductivities of the inner and outer material are $k^{inner} = 40 \text{ W}/(\text{m}^\circ\text{C})$ and $k^{outer} = 20 \text{ W}/(\text{m}^\circ\text{C})$. The target values are temperatures on three characteristic radii: inner, interfacial and outer, which are $T_A = 25.06^\circ\text{C}$, $T_B = 17.84^\circ\text{C}$ and $T_C = 13.16^\circ\text{C}$, respectively.

Only one–eighth of the hollow sphere is presently analyzed due to the symmetry. The finite element configurations used were HC8/9, HC8/15, HC8/27, HC20/21 and HC20/27, and raw primal one H8. The sequence of models with uniform meshes refinement in all directions, were investigated. The coarsest mesh is shown in Fig. 8. Relative errors of calculated temperatures on three characteristic radii versus the number of finite elements in the mesh, are shown in Fig. 8.

The results reported in Fig. 8, reveal that all considered finite element configurations have high accuracy. In addition, artificially enforced continuity of heat flux shape functions along discontinuity surface of the abrupt material change (Point B) does not deteriorate results. Nevertheless, quadratic finite element configurations H20, H20/21 and H20/27 have relative error less than 0.01% immediately after the second discretization, which points out to the high accuracy of these configurations.

Let’s investigate whether level of mesh refinement in radial direction influences results. It will be done on a sequence of models, which have fixed number of elements along circumference, namely, 48 finite elements. Meshes are gradually refined in radial direction only, with mesh indicators $M + N$, per inner and outer materials of the sphere respectively, where $M = 3, \dots, 7$ and $N = 2, \dots, 6$. For this type of discretization relative percentage errors are shown in Fig. 9.

From results reported in Fig. 9, it can be seen that all considered finite element configurations retain the same level of accuracy during the mesh refinement process, even on the material interface. It can be seen that very good results are obtained even with small number of elements in radial direction. Therefore, we may say that level of mesh refinement in radial direction does not affect results. Further, the time efficiencies, i.e. execution time versus number of degrees of freedom, of HC8/9 finite element configuration (see Fig. 8) in connection with several presently considered solution schemes, are shown in Fig. 10.

From results reported in Fig. 10, it can be seen that MA47+MC30 procedure [5] is far more time efficient than other presently considered solution procedures, i.e. it is 50 times faster than simple Gaussian elimination procedure and 25 times faster than MA47 procedure, on the same computer platform.

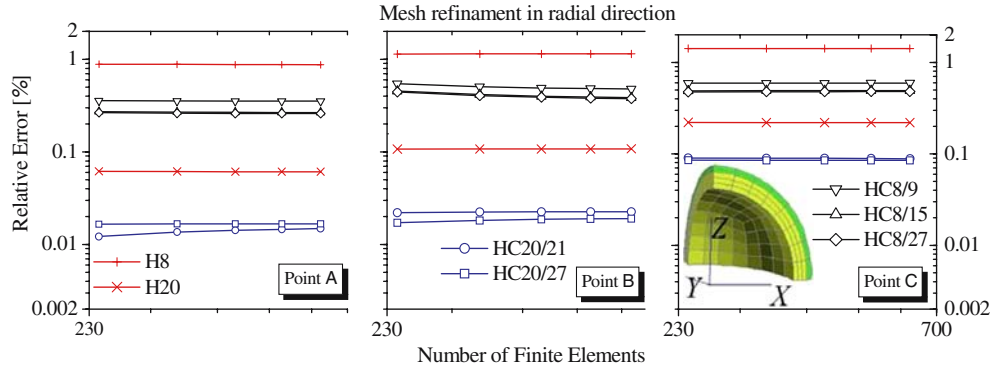


Fig. 9 Hollow sphere – uniform refinement: relative errors

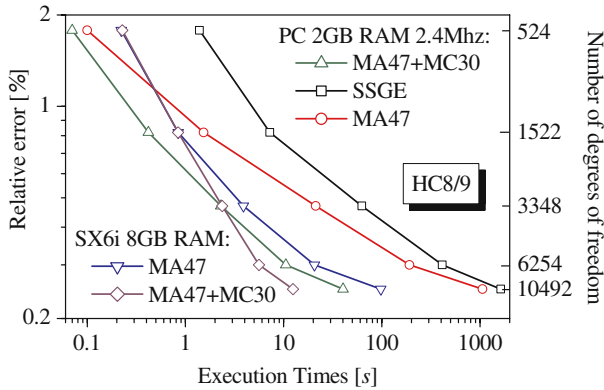


Fig. 10 Hollow sphere – radial refinement: relative errors

7.2 Cylinder with prescribed heat flux

Performance of the present approach in the presence of non-smooth heat flux boundary conditions is presently investigated. The model problem is a cylinder [24], shown in Fig. 11, with thermal conductivity $k = 52 \text{ W}/(\text{m}^\circ\text{C})$ and prescribed heat flux $h = 5 \cdot 10^5 \text{ W}/(\text{m}^2\text{C})$ along CE strip on its side surface. The bottom is maintained at fixed zero temperature. Top side and side strip BE are insulated. The target value is

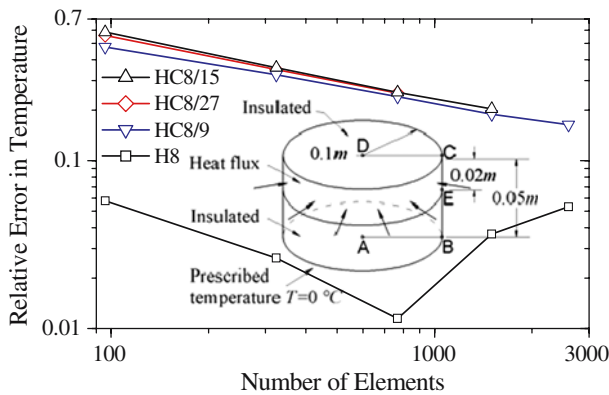


Fig. 11 Hollow sphere: time efficiency

temperature at point E on discontinuity line, where $T(E) = 213.6^\circ\text{C}$ [24]. One-quarter of the cylinder is analyzed due to the symmetry. The convergences of the results obtained by the raw primal H8, and present HC8/9, HC8/20 and HC8/27 finite element configurations, are shown in the Fig. 11

It can be seen in Fig. 11 that all considered FE configurations have relative errors in temperature less than 1%. In addition, for the present finite element configurations there are no oscillations of the results during mesh refinement process, regardless of the enforced continuity of the heat flux shape functions over the line of heat flux boundary conditions discontinuity. Therefore, we may conclude that this enforced continuity does not deteriorate temperature result in any way. However, unlike in previous example of the hollow bimaterial sphere, where the present scheme is more accurate than primal H8, in the present example it is “less” accurate. Nevertheless, it does not oscillate, as primal one. So, ultimately, its performance is again better than of primal scheme.

It should be noted that all above observations are valid for primal variable only, that is, temperature. The lack of target solution for dual (heat flux) variable, disables us to measure convergence of the results per heat flux variable, which will be particularly interesting because heat flux is calculated a posteriori in primal approach. Nevertheless, the visualization of the heat flux component q^z for the model with 1,500 finite elements, discretized by finite element HC8/9, primal HEXA8 [25] without and with heat flux averaging, are shown in Fig. 12, respectively.

In the present approach, the heat flux boundary conditions on the upper side of the cylinder are prescribed to be zero and introduced in the calculation as homogenous essential boundary conditions. It is unlike in primal schemes, where prescribed heat flux components can not be applied, which results in some artificial “small” value of a posteriori calculated heat flux field.

7.3 Thermal barrier coating component

A hollow long steel shaft coated by a bond and a ceramic layer [26] shown in Fig. 13, is analyzed. The inner and outer radii of the shaft are $r_3 = 0.005 \text{ m}$ and $r_0 = 0.1 \text{ m}$, respectively.

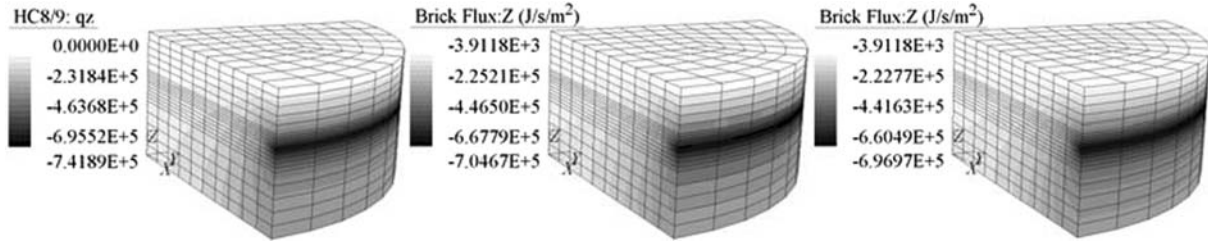


Fig. 12 Cylinder with prescribed heat flux: relative errors in temperature

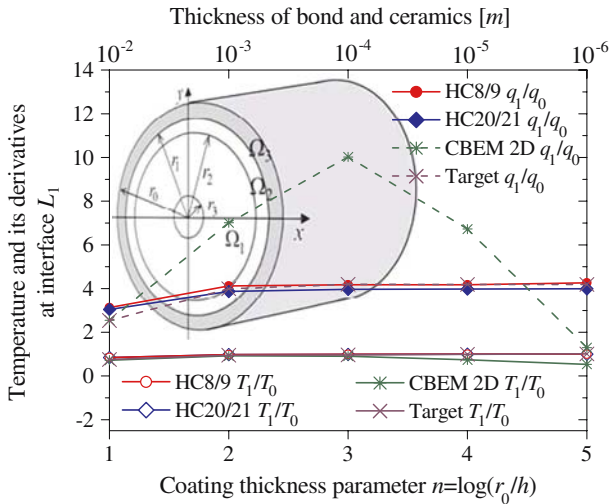


Fig. 13 Cylinder with prescribed heat flux: visualization of the heat flux component q_z

It is assumed that shaft’s height is $h = 0.1$ m. Thermal conductivity of steel and bond is $k = 25$ W/(mK), while thermal conductivity of the ceramic is $k = 1$ W/(mK). The temperature is prescribed on the inner and outer surfaces, such that $T_3 = 500^\circ\text{C}$ and $T_0 = 1000^\circ\text{C}$, respectively. Five models with decreasing thickness of coating t , that is, of bond and ceramic together, varied from $10^{-2} - 10^{-6}$ m, are analyzed.

One-quarter of the cylinder is analyzed due to the symmetry. All five model problems are discretized by eight finite elements along circumference, and only one layer of finite elements along the height. The radial meshing is performed by gradual refinement toward coating. Both, bond and ceramic regions are discretized by at least three finite element layers, along radius. Number of finite elements for five considered model problems with decreasing coating’s thickness, is 120, 160, 192, 248 and 384, respectively. The results obtained by finite element configurations HC8/9 and HC20/21 are compared with results obtained by two-dimensional conventional boundary element approach (CBEM) [26] and analytical result. Non-dimensional temperature T_1/T_0 and radial heat flux component q_1/q_0 , versus non-dimensional coating thickness $n = \log(r_0/t)$, are given in Fig. 13.

From Fig. 13, it can be seen that the present approach shows excellent agreement with analytical solution, while CBEM exhibits spurious behavior. Execution times on PC

1 GB RAM, 2.4 MHz for all model problems, are in range from 0.32 to 25.72 s. The same level of accuracy is obtained in the subsequent primal-mixed thermal stress analysis. Therefore, present approach can be a useful tool for the coating design and peeling-off failure analysis of thermal barrier coated components.

7.4 Transient temperature distribution in an orthotropic metal bar

Transient heat transfer in a long metal bar [27,28] with rectangular cross-section shown in Fig. 14, is analyzed. The material is orthotropic, with thermal conductivities: $k_x = 415.03$ W/m°C, $k_y = 74.78$ W/m°C and $k_z = 20.75$ W/m°C. The specific heat is $c = 534.53$ J/kg°C, density $\rho = 6407.38$ kg/m³. The bar is exposed to convection, with convection coefficient $h_c = 196079.05$ W/m°C and ambient temperature of $T_a = 37.78^\circ\text{C}$. Initial temperature of the body is $T_0 = 148.89^\circ\text{C}$. The length of the bar is $l = 0.008382$ m, although it does not influence the temperature results. Target values are temperatures at four points in the corners at the end of the time interval of 3 s [28]. Suggested time step size for this model was $\Delta t = 3/40$ s. Nevertheless, in order to prove the stability of the present time integration scheme, much larger time step sizes were considered.

One quarter of the model problem is analyzed due to the symmetry. Convergence at the node N2 with extremal

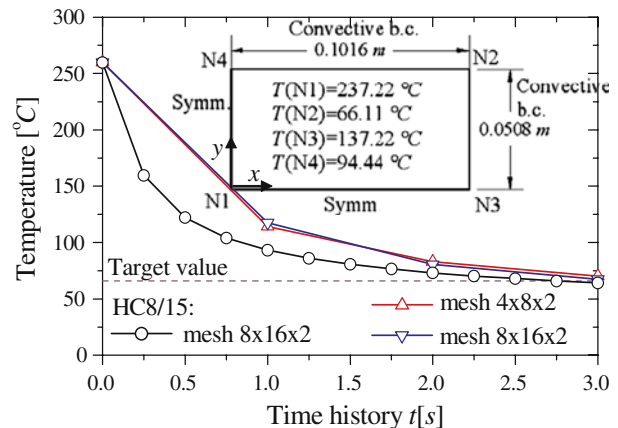


Fig. 14 Coated model: temperature and heat flux per coating thickness parameter

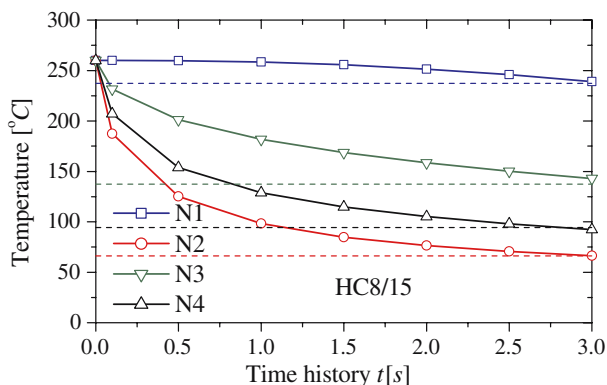


Fig. 15 Orthotropic bar: time convergence at node N2

temperature value, for larger and smaller time steps, are shown in Fig. 14. The convergence at all corner nodes, are shown in Fig. 15

The present approach converges to the target values regardless of the size of the time step. Presently, we have obtained target results with only few time steps, unlike in [28] where 40 time steps were recommended for the given time interval.

7.5 Transient heat conduction with heat generation

Transient heat transfer within a plane wall [23,24] shown in Fig. 16, subjected to the internal heat generation $f = 50 \text{ MW/m}^3$, is presently analyzed. Material properties are: thermal conductivity $k = 19 \text{ W/(mK)}$, specific heat $c = 460 \text{ J/kg K}$ and density $\rho = 7800 \text{ kg/m}^3$. The initial temperature of the wall is $T_0 = 373 \text{ K}$. The wall is subjected to convection on the sides A–C and B–D, where $h_c^{AC} = 400 \text{ W/m}^2 \text{ K}$, $T_a^{AC} = 393 \text{ K}$, $h_c^{BD} = 500 \text{ W/m}^2 \text{ K}$ and $T_a^{BD} = 293 \text{ K}$. Target value is temperature at the point E after period of 9 s: $T^E|_{t=9s} = 463.7033 \text{ K}$. Suggested number of time steps in reference [25] is 100, giving us time step of $\Delta t = 0.09s$. The finite element configurations HC8/9 and

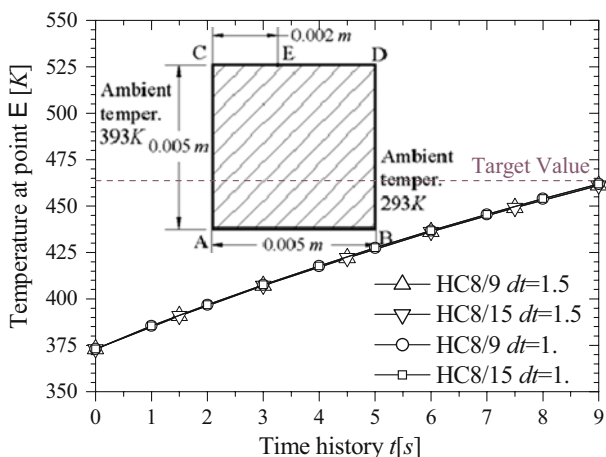


Fig. 16 Orthotropic bar: time convergence at target nodes

HC8/15, and much smaller sizes of time step, are presently considered.

We can conclude that both presently considered finite element configurations, HC8/9 and HC8/15, converge to the target result for much smaller number of time steps than recommended in [25], which significantly reduces the time needed for calculations.

8 Conclusion

The fully three-dimensional primal–mixed finite element approach in steady–state and transient heat transfer analysis of the solid body, is examined in detail. Both solution variables: temperature and heat flux, are simultaneously calculated from the same system of equations. As a novelty, the interelement continuity of heat flux shape functions is intentionally enforced. It is observed that it does not deteriorate temperature and heat flux target results even in the region of some kind of discontinuity. The mathematical aspects of convergence of the proposed finite element family HCT/q , is carefully analyzed also. It is proven that present hexahedral finite element configurations HC8/9, HC8/15, HC8/27, HC20/21 and HC20/27 are consistent, solvable, and satisfy the first stability condition. In addition, finite element HC8/27 satisfies second stability condition, also. Therefore, it is proven that present finite element HC8/27 is *reliable*. Further, obtained solutions converge to the target result, regardless of the complexity of the geometry, presence of the abrupt material changes, non-smoothness of heat flux boundary conditions or distortion of the finite element mesh. Nevertheless, one of the main potentials of the present approach is in overcoming of the well-known transition problem of connecting finite elements of different types and dimensions. Consequently, present finite elements are robust even in micron–sized coated components analysis. In addition, in connection with specially designed HSL solution routine MA47+MC30, the present finite element approach is time efficient, measured as the accuracy versus the solution time. It is shown that in comparison to primal *raw* finite element approach and classical boundary element approach, the present scheme is more robust and accurate. Finally, the present approach can be easily implemented in any existing pre and postprocessing environment developed for primal finite element approach, as it is presently implemented in Straus7 [25] software package.

Acknowledgements The authors would like to acknowledge support from Ministry of Science and Environmental Protection of Republic of Serbia (www.mntr.sr.gov.yu) for providing financial support for this research under the grant IO1865. In addition, the authors express gratitude to NEC (www.nec.com) for the opportunity to work on SX6i supercomputer in performance assessment scheme. Also, we are grateful to Professor Iain Duff from CCLRC Rutherford Appleton Laboratory (www.cse.clrc.ac.uk) and his support in the use of the state-of-the-art HSL routines. Finally, we are grateful to Japan–Serbia & Montenegro Center for Simulation Science (www.center.bg.ac.yu/simulation/), where we conducted most of our numerical experiments on NEC SX6i supercomputers.

References

1. Russell MB, Probert SD (2004) FDiff3: a finite-difference solver for facilitating understanding of heat conduction and numerical analysis. *Appl Energy* 79:443–456
2. Bathe KJ (1996) *Finite element procedures*, Prentice hall, Englewood Cliffs
3. Zienkiewicz OC, Taylor RL (2000) *The finite element method – the basis*. Butterworth–Heinemann, London
4. Arnold DN (1990) Mixed finite element methods for elliptic problems. *Comput Methods Appl Mech Eng* 82:281–300
5. Duff IS, Reid JK (1983) The multifrontal solution of indefinite sparse symmetric linear systems. *ACM Trans Math Softw* 9(3):302–325
6. Reid JK, Duff IS (1995) MA47, a Fortran code for direct solution of indefinite sparse symmetric linear systems. Rep RAL-95-001
7. Arjunon S, Richardson JD (2005) Regularized p-version collocation BEM algorithms for two-dimensional heat conduction. *Eng Anal Bound Elem* (in press)
8. Wang H, Qin QH, Kang YL (2005) A meshless model for transient heat conduction in functionally graded materials. *Comput mech* (in press)
9. Liu Y, Zhang X, Lu M (2005) Meshless least-squares method for solving the steady-state heat conduction equation. *Tsinghua Sci Tech* 10:61–66
10. Quarteroni A, Sacco R, Saleri F (2000) *Numerical Mathematics*. Springer, Berlin Heidelberg New York
11. Burgess G, Mahajerin E (2003) Transient heat flow analysis using the fundamental collocation method. *Appl Therm Eng* 23:893–904
12. Fung TC (2000) Unconditionally stable higher-order accurate collocation time-step integration algorithms for first-order equations. *Comput Methods Appl Mech Eng* 190:1651–1662
13. Brezzi F, Fortin M, Marini D (1993) Mixed finite element methods with continuous stresses. *Math Models Meth Appl Sci* 3(2):275–287
14. Bathe KJ (2001) The inf-sup condition and its evaluation for mixed finite element methods. *Comput Struct* 79:243–252
15. Hinton E, Campbell JS (1974) Local and global smoothing of discontinuous finite element functions using a least squares method. *Int J Num Methodss Eng* 8:461–480
16. Mijuca D (2004) On hexahedral finite element HC8/27 in elasticity. *Comput Mech* 33(6):466–480
17. Miranda S, Ubertini F (2001) On the consistency of finite element models in thermoelastic analysis. *Comput Methods Appl Mech Eng* 190:2411–2427
18. Duff IS, Gould NI, Reid JK, Scott JA, and Turner K (1991) Factorization of sparse symmetric indefinite matrices. *IMA J Numer Anal* 11:181–204
19. Olson MD (1983) The mixed finite element method in elasticity and elastic contact problems. In: Atluri SN, Gallagher RH, Zienkiewicz OC (eds) *Hybrid and mixed finite element methods*. Wiley, New York pp 19–49
20. Kasper EP, Taylor RL (1997) A mixed-enhanced strain method: linear problems. University of California, Report No.UCB/SEMM-97/02
21. Micheletti S, Sacco R (2001) Dual-primal mixed finite elements for elliptic problems. *Numer Methods Partial Diff Equat* 17:137–151
22. Berkovic M, Mijuca D (1999) On the main properties of the primal-mixed finite element formulation. *Facta Universitatis Series Mechanics, Autom Control and Robot* 2:903–920
23. Lewis RW (1990) First 3-D heat transfer benchmarks completed. Benchmark, New York pp 9–12
24. G+D Computing Straus7, Finite element analysis system software package – Verification Manual. www.strand.aust.com, Australia
25. Mijuca D, Drašković Z and Berković M (1996) Displacement based stress recovery procedure. *Advances in finite element technology, Civil-Comp Press*, pp 127–134
26. Societe Francaise des Mecaniciens (1989) Commission Validation des progiciels de calcul de Structures, groupe de travail thermique (2D et 3D) et thermoelasticite TPLV 04/89. Paris
27. Standard Benchmark examples. NAFEMS, BMTTA (S), No. 15(i)
28. Lu S, Dong M (2003) An advanced BEM for thermal and stress analyses of components with thermal barrier coating. *Electron J Bound Elem* 1:302–315
29. Schneider P J (1957) *Conduction heat transfer*, 2nd printing. Addison-Wesley, Reading, MA
30. Verification Manual. ANSYS Inc., www.ansys.com, US
31. Holman JP (1990) *Heat transfer*. McGraw-Hill, New York